Progress Toward Charge Exchange Experiments in a Mini-Electron Beam Ion Trap Using Transition Edge Sensors

Adrika Dasgupta, Jonathan W. Dean, Galen O'Neil, Nathan Nakamura, Joel Weber, Kelsey Morgan, Yuri Ralchenko, Daniel Swetz, Joseph N. Tan, Noah W. Zuckman, and Fabian Kislat

***Abstract*—Charge exchange is a process observed where highly charged ions interact with neutral atoms or molecules, capturing electrons and emitting X-rays as the excited states decay toward the ground state. Charge exchange-induced X-rays provide information on the ion composition, temperature, and density of high-temperature plasmas. Accurate charge exchange cross section data from ground-based laboratory experiments are required to interpret the charge exchange-induced X-ray emissions observed in astrophysical and laboratory plasma environments. In this work, we describe the development of a laboratory setup, a 0.7 T miniature-Electron Beam Ion Trap (mini-EBIT), for studying charge exchange interactions between highly charged neon ions and neutral gases (H or He), using a transition-edge sensor (TES) microcalorimeter array. We have designed and built a cost-effective pulsed gas injection system to introduce short, well-defined pulses of neutral gas into the EBIT to better model charge exchange events and to provide precise timing control. Detailed information about the characteristic emission lines of the neon ions would allow accurate determination of the cross sections involved in charge exchange processes. We present the initial results obtained from the mini-EBIT using this advanced TES detector array. We will also present time-of-flight spectra from a microchannel plate time-of-flight detector, as well as X-ray emission lines from a silicon drift detector, to characterize the highly charged ion production in the mini-EBIT.**

***Index Terms*—Charge exchange, electron beam ion trap (EBIT), highly charged ions, microcalorimeter, pulsed gas injection system, transition-edge sensor (TES), X-ray spectra.**

Received 24 September 2025; revised 30 March 2026; accepted 2 April 2026. Date of publication 8 April 2026; date of current version 24 April 2026. This work was supported in part by the U.S. Department of Commerce through the National Institute of Standards and Technology under Award 70NANB23H027, and in part by the University of New Hampshire group through NSF RII Track-4 under Award 2132167. *(Corresponding author: Adrika Dasgupta.)*

Adrika Dasgupta and Fabian Kislat are with the University of New Hampshire, Durham, NH 03824 USA (e-mail: Adrika.Dasgupta@unh.edu).

Jonathan W. Dean is with the University of Colorado, Boulder, CO 80309 USA, and also with the National Institute of Standards and Technology, Boulder, CO 80305 USA.

Galen O'Neil, Nathan Nakamura, Joel Weber, Kelsey Morgan, and Daniel Swetz are with the National Institute of Standards and Technology, Boulder, CO 80305 USA.

Yuri Ralchenko and Joseph N. Tan are with the National Institute of Standards and Technology, Gaithersburg, MD 20899 USA.

Noah W. Zuckman is with Colorado State University, Fort Collins, CO 80523 USA.

Color versions of one or more figures in this article are available at https://doi.org/10.1109/TASC.2026.3682138.

Digital Object Identifier 10.1109/TASC.2026.3682138

I. Introduction

CHARGE exchange, or charge transfer, is a process wherein an ion and a neutral atom in close proximity have one or more electrons jump from one to the other.

The process is represented by

$$X^{q+} + N = X^{(q-m)+} + N^{m+} \tag{1}$$

where X is the ion, q is the initial ion charge, N is the neutral atom, and m is the number of electrons captured. The captured electrons initially populate the excited bound-states, which cascade into lower states and eventually to the ground state, emitting photons at each step. The maximum populated energy level ($n_{\max}$) after the interaction is given by [1]

$$n_{\max} = q\left[1 + \frac{q-1}{\sqrt{2q}}\right]^{-1/2}. \tag{2}$$

As charge exchange populates higher energy levels in the capturing ion than other excitation mechanisms, the X-ray spectrum produced in the charge exchange process is different from those produced in other processes. Charge exchange cross sections, on the order of 10^{-15}–10^{-14}cm^2, are significantly larger than that of other atomic processes, such as collisional ionization and electron impact excitation, which typically range from 10^{-17} to 10^{-16} cm^2 under comparable conditions [2], [3], [4], [5]. This highlights why charge exchange often dominates in environments where highly charged ions interact with neutral species.

Charge exchange is a common process in many astrophysical environments, especially where hot, ionized plasma meets cold, neutral gas. The first astrophysical evidence was from observations of the comet Hyakutake in 1996 [6], [7]. Since then, charge exchange has been identified to play a significant role in other astrophysical objects, such as planetary magnetospheres, where ions from the solar wind interact with neutral atoms in the planet's atmosphere [8], [9]; in galaxies [10], [11], including our own Milky Way [12]; in the interstellar medium [13]; in supernova remnants, where fast-moving ions collide with surrounding material [14]. Beyond astrophysics, charge exchange is important for fusion research devices, such as tokamaks and stellarators, to diagnose plasma properties [15], [16].

To utilize charge exchange spectral features as a plasma diagnostic tool in astrophysical and fusion plasmas, an understanding of the charge exchange cross sections and the excited energy

levels that are populated during the interaction is required. State-selective charge exchange cross sections, which describe the probability of an electron capture in a specific quantum state, and line intensities can be predicted by existing theoretical models. In ground-based laboratory experiments, X-ray spectra from the charge exchange interactions between highly charged ions and neutral atoms can be studied in controlled settings. This helps to refine the theoretical models, providing reference data necessary for interpreting the observations. These lab-based studies also support missions, such as X-Ray imaging and spectroscopy mission (XRISM) [17], [18] and the proposed NewAthena [19], [20], by helping us analyze their X-ray data effectively.

Over the years, various experimental approaches have been used to study charge exchange in laboratory settings, depending on the ion-neutral collision velocity regimes. Laboratory experiments, particularly from the 1950s, focused on crossed-beam and merged-beam techniques to investigate charge exchange processes at intermediate/ high ion-neutral collision velocities ($>10^7$ cm/ s) where the charge exchange cross section is generally low but important in certain energetic astrophysical and fusion plasmas. In the 1990s, electron beam ion traps (EBITs) were developed for lower collision velocities ($< 10^6$ cm/ s) where charge exchange becomes much more probable due to higher cross sections [2].

II. Miniature-EBIT

The miniature-Electron Beam Ion Trap (mini-EBIT, Fig. 1) at the National Institute of Standards and Technology (NIST), Boulder campus, is a compact and cost-effective alternative [21] to the larger EBIT built at NIST, Gaithersburg campus, in 1993 [22]. However, the production of a wide range of highly charged ions is not achieved to the same extent with the mini-EBIT as with the EBIT at Gaithersburg.

The mini-EBIT is designed to create highly charged states of ions using an electron beam and trap them using a combination of electrostatic potential and magnetic field. The electron beam of diameter 6.35 mm is generated by thermionic emission from a heated tungsten filament and can be accelerated up to an energy of 5 keV, allowing it to fully strip argon [23]. The beam is directed toward the anode and then focused by a set of electrodes with controlled voltage differences into the central region where gas is injected, ionized, and trapped. Highly charged ions are created by electron impact ionization when a neutral gas is injected into the main chamber and exposed to an electron beam. Radial trapping of ions is achieved by the space charge of the electron beam, combined with a strong magnetic field of approximately 0.7 T generated by permanent NdFeB magnets inside the mini-EBIT. Axial trapping is provided by the electrostatic potential between the electrodes. The electrode located at the center of the main chamber is called the middle drift tube. The two electrodes surrounding the trap region are known as endcap electrodes and are set to a higher voltage than the middle drift tube, to form a potential well that longitudinally traps ions between the two endcaps. Typically, the middle drift tube is 20–30 V below the endcaps with all other voltages of the order 200–5000 V.

The internal components of the mini-EBIT are seen in Fig. 1(b). The system is operated at ultra-high vacuum

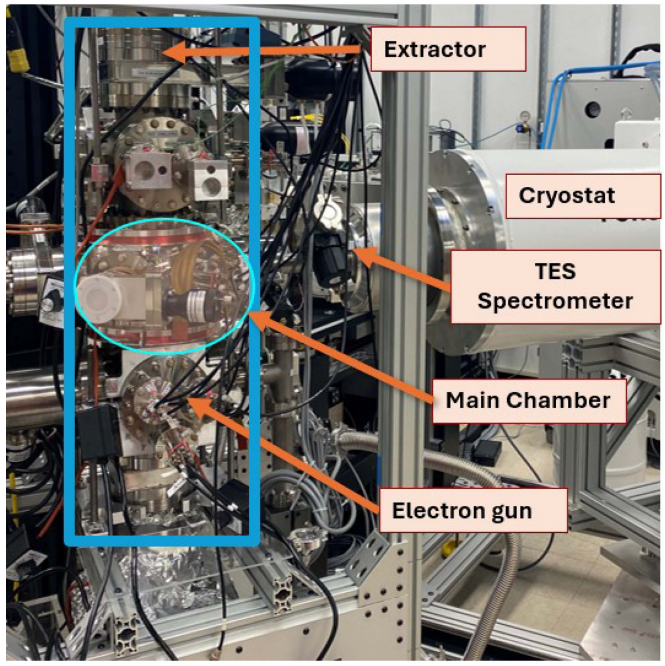

(a)

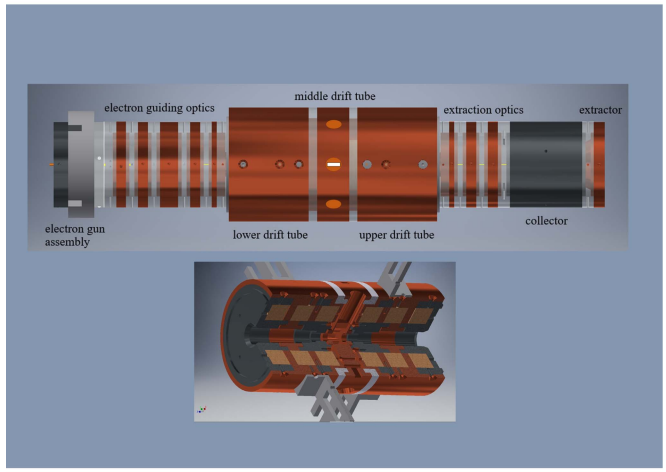

(b)

Fig. 1. In total, 0.7 Tesla, room-temperature, miniature-Electron Beam Ion Trap (mini-EBIT) at the NIST. (a) Photograph of the experimental setup with the EBIT light source docked to TES spectrometer inside the cryostat. (b) Schematic representation of the mini-EBIT electrode stack rotated 90° from the vertical, with a quarter-cut inset showing six embedded rings of radially polarized NdFeB magnets. The electron beam is generated by a dispenser cathode, and focused to propagate through the magnetized drift tubes. The middle drift tube, where the ions are created and trapped, has six equidistant slits to allow gas injection for charge exchange experiments, and light collection by the detectors perpendicular to the chamber.

($\sim 10^{-7}$Pa), which helps to reduce unwanted collisions with the background inside. The base pressure in the main chamber is 2.66×10^{-7} Pa (2nTorr), and during gas injection increases to between 1.33×10^{-6} Pa (10nTorr) and 6.65×10^{-5} Pa (500 nTorr).

For the gas injection system, a needle valve is used to regulate the pressure in an initial volume, which is connected to an intermediate chamber by a pinch-off tube. This intermediate chamber is continuously pumped by a turbo pump to maintain

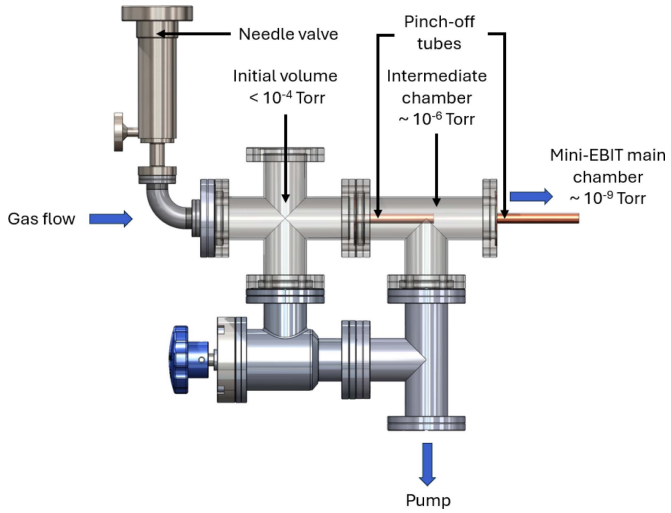

Fig. 2. Schematic of the continuous gas injection system. Direction of gas flow, connection to the vacuum pump, and the mini-EBIT main chamber are indicated by the blue arrows. Gas is injected into the initial volume regulated by the needle valve, passes through the intermediate chamber, and enters the mini-EBIT main chamber via the pinch-off tubes.

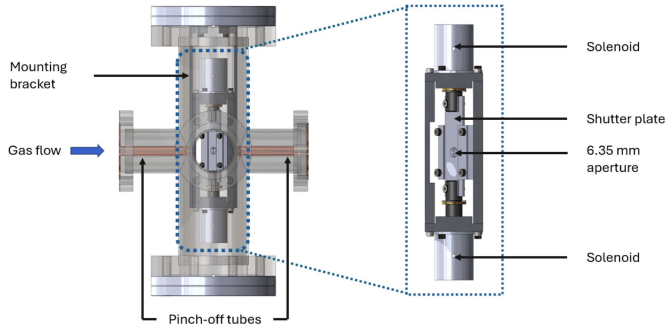

Fig. 3. Schematic of the designed pulsed gas injection system. The two opposing solenoids actuate the shutter plate. The entire assembly is supported by custom-made parts and mounted inside a vacuum chamber using the mounting brackets. The alignment of the aperture on the shutter plate with the mounting brackets allows the gas flow to the mini-EBIT.

$\sim 10 \times 10^{-6}$ Torr pressure and connected to the main chamber with a second pinch-off tube. This two-tube arrangement ensures a ballistic injection of gas into the main chamber (see Fig. 2). Scattered gas molecules that are not directed toward the trap region are effectively removed in the intermediate chamber.

A second low-cost pulsed-gas injection mechanism (see Fig. 3) has been developed with modifications to the existing continuous gas injector system. This includes a shutter in between the two 6.35 mm diameter pinch-off tubes in the intermediate volume for short, well-timed, pulses of neutral gas. The system consists of two custom-made vacuum-compatible pull-type solenoids attached to a plate with 6.35 mm aperture that acts as the fast shutter. Energizing one solenoid pulls the shutter open, while the other pulls it closed. This allows the injection of very short ($\sim$20 ms) puffs of neutral gas into the trap region. The pulsed gas injection system has advantages over a continuous flow scheme, such as improving the signal-to-background ratio in X-ray measurements, enabling time-selective sampling, and maintaining a consistent neutral gas density [24], [25]. This ensures that the detected X-rays originate specifically from charge exchange between the highly charged ions and the neutral gas, and helps isolate spectral features within the narrow time window of the interaction.

There are several detectors that gather information on the processes occurring in the main chamber. A time-of-flight (TOF) detector is used to investigate the specific ions being created. During the ion trapping, the middle drift tube potential is set lower than the lower and the upper drift tube to form a potential well, confining the ions after cooking them for typically (100–300 ms). The middle drift tube potential then briefly switches to a higher value than the upper drift tube to release the trapped ions, which are accelerated toward an extraction electrode with a potential of -1200 V. The extraction electrode is located at the end of the electrode sequence, as shown in Fig. 1(b). The microchannel plate (MCP) of the TOF detector is an electrode at an even lower potential, typically -2050 V, accelerating the ions onto it. The timing between the trigger when the ions are extracted from the trap and the current received when the ions arrive at the TOF microchannel is measured, providing information on the specific ions' TOF. The charge states of the ions that are trapped in the main chamber can be determined by analyzing this TOF data.

Two X-ray detectors are attached to the mini-EBIT. First, a silicon drift detector (SDD) is attached to the mini-EBIT and provides 50–100 eV resolution for X-rays in the 300 eV to 3.5 keV range. Second, superconducting transition edge sensor (TES) microcalorimeters have been included to capture high-resolution X-ray spectra [26]. The TES resolution is of order 1 eV, far superior to the SDD, and enables greater understanding of the processes creating the observed X-rays. The complete TES detector assembly [see Fig. 4(a)], including 252 TES detector pixels and readout electronics, is housed within a cryostat that integrates with the mini-EBIT chamber. Each TES is a molybdenum/gold bilayer consisting of a 30 μm $\times$ 90 μm patch of gold (Au) with two parallel, 7 μm wide, molybdenum (Mo) strips underneath. The TES is adjacent to 250 μm $\times$ 250 μm $\times$ 250 nm Au absorbers [see Fig. 4(b)]. Above the array is an aperture with each opening 200 μm $\times$ 200 μm wide, ensuring photons are only incident upon the absorbers. The critical temperature of the TES is 55 mK, and the bath temperature is 21 mK. More details on a similar TES array are given in [27].

III. Preliminary Results

The main objective is to study the interaction of highly charged neon (Ne) ions with neutral helium (He) gas. Neon is a common element in the solar system, making these interactions potentially interesting for astrophysical plasmas. The ionization potential of H-like Ne (Ne^{9+}) is 1362 eV [23], well within the capabilities of the mini-EBIT. Preliminary results have been obtained for Ne ions in the mini-EBIT.

A. TOF Detector

To identify the ions present in the mini-EBIT, TOF spectra were obtained using the MCP TOF detector. The TOF detector

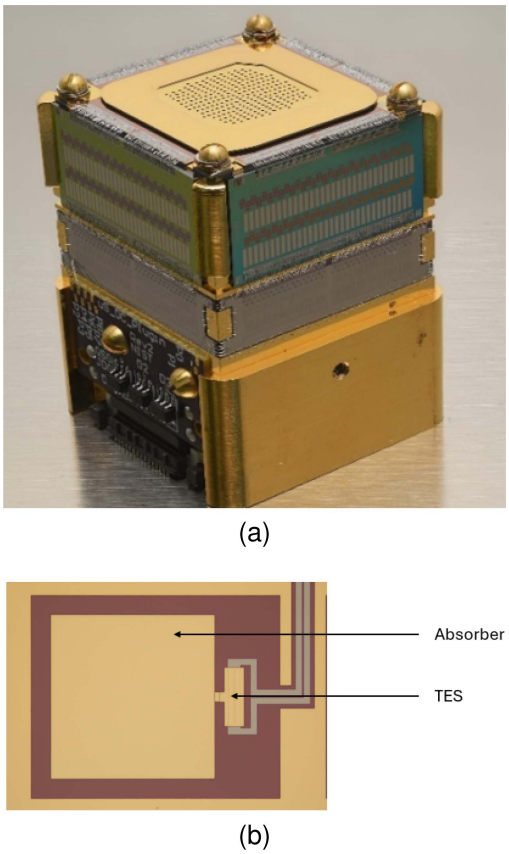

Fig. 4. (a) Complete TES detector assembly with the TES array at the center and the readouts on the sides for the mini-EBIT. (b) Schematic of "sidecar style" absorber structure, where the 250 μm $\times$ 250 μm $\times$ 250 nm Au absorbers are placed next to the Mo/Au TESs.

measures the time (t) required by each HCI to travel from the Extractor electrode to the detector. During this process, the ions are accelerated mostly in a constant electric field, and their time of arrival depends on their mass-to-charge ratios (m/q)

$$t \approx k\sqrt{m/q} \tag{3}$$

where t is the TOF, k is an instrument-dependent constant determined by the extraction voltage and the distance between the extractor and the detector, and m and q are the mass and charge of the ions, respectively. Since different ions with the same m/q ratios have identical flight times and show up on the same peak, this causes ambiguity in the definitive identification of the peaks. Therefore, the ions present are predicted based on the analysis of the entire spectrum and the known gases introduced into the system.

A TOF spectrum during Ne injection is given in Fig. 5. The *X*-axis of the TOF spectrum represents the TOF (ms), while the *Y*-axis represents the ion signal intensity (V). The first (leftmost) peak represents hydrogen ions (protons), which have the lowest mass-to-charge ratio with $m/q = 1$. The second peak is due to the fully stripped ions with $m/q \approx 2$. These two peaks are used as calibration lines for the TOF spectrum to predict the other peaks. For instance, in the case of Fig. 5, the nine individual charge states of Ne are predicted. There is good evidence that Ne of all charge states up to and including Ne^{6+} have been created, and future work will involve altering the beam state, gas pressure, and beam energy to obtain higher charge states.

B. Silicon Drift Detector

When studying the charge exchange phenomenon, it is essential to obtain both X-ray spectroscopy and charge state measurements for a comprehensive analysis of the underlying mechanisms. As described in the previous section, charge state information can be provided by measuring the TOF of ions extracted from the mini-EBIT, guided to a fast MCP ion detector. In this section, we present observation of X-ray emissions by ions produced in the mini-EBIT using an SDD with 25 mm^2 active area and a silicon nitride window.

The first peak from the SDD spectra in Fig. 6 shows He-like carbon (C^{4+}) transitions around 304 eV. The second peak corresponds to the He-like oxygen (O^{6+}) transitions around 568 eV. In the low energy regime, the energy resolution of the SDD from AmpTek is 60 eV, which is better than the its specification of 123 eV FWHM for Mn (Kα) at 5.9 keV. Nevertheless, much higher resolution would be needed to observe the well-known transitions—resonance (W), intercombination (X,Y), and forbidden (Z) lines—of highly charged He-like ions, or the Lyman series of H-like ions. In the dominant peaks centered around 914 and 1021 eV, however, the better-than-specified resolution of this SDD is barely adequate to resolve the He-like (Ne^{8+}) and H-like (Ne^{9+}) neon X-ray emissions at electron beam energies approaching 4.5 keV. The peaks at higher energies have not been identified yet but is assumed to be due to the presence of tungsten or gold inside the mini-EBIT.

Although SDDs are favored for their user-friendly nature and ability to operate at room temperature, their energy resolution is generally not sufficient to resolve closely positioned X-rays. As a result, the individual transitions of interest in the peaks corresponding to Ne^{8+} and Ne^{9+} could not be distinguished in the spectrum.

C. Transition Edge Sensors

The TES detectors are known for their exceptional energy resolution, which helps to clearly differentiate closely spaced X-ray lines [26] corresponding to specific charge states of neon (Ne^{9+}, Ne^{8+}, etc.).

Fig. 7 compares the X-ray spectrum collected with the TES spectrometer using a copper (Cu) calibration source to the spectrum observed when injecting neon gas into the mini-EBIT. With neon injection, the SDD detects a clear neon peak, confirming the presence of neon in the mini-EBIT. However, in the TES spectrum, the corresponding peak could not be confirmed as neon with neon injection due to an overlap with the Cu Lα line. This Cu line is assumed to originate from the electrodes inside the mini-EBIT and was present even when the external Cu calibration source, an X-ray tube with a Cu anode operating between 5 and 7 kV, was OFF. Since the SDD and the TES spectrometer are attached to two different ports on the mini-EBIT, and the Cu surfaces inside the chamber are not symmetric, we suspect

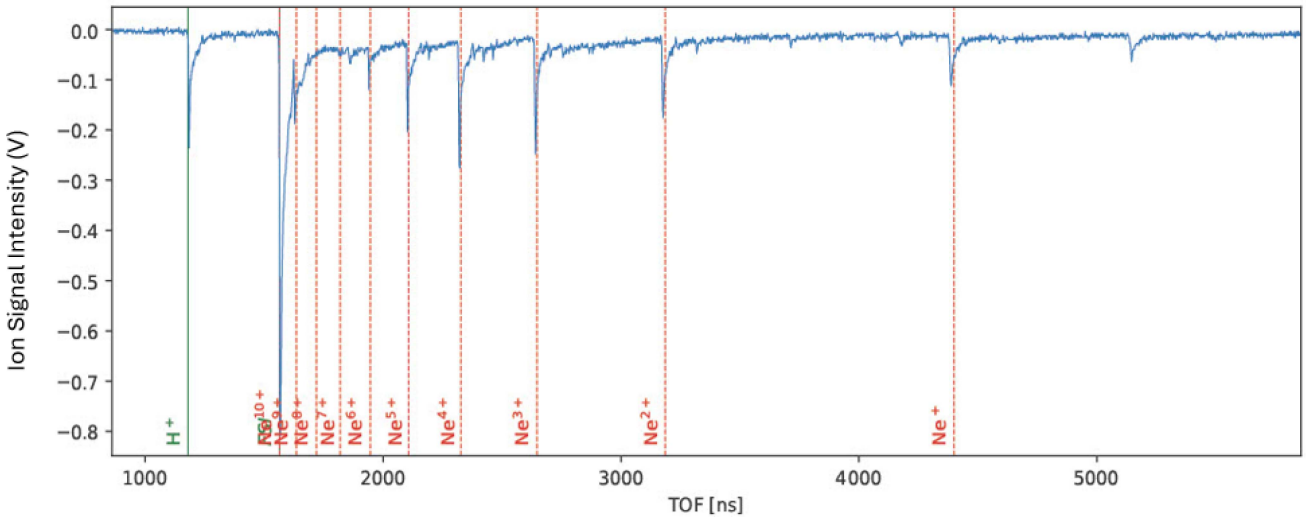

Fig. 5. TOF spectrum showing different Neon ions possibly present inside the mini-EBIT. This spectrum was obtained after cooking the ions for 300 ms with an electron beam of energy 3 keV and 1.4 mA electron beam current.

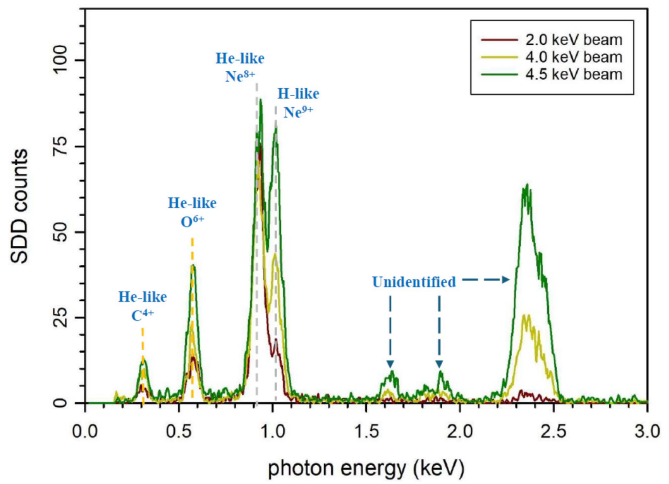

Fig. 6. SDD spectra obtained with 30 min integration time, for electron beam energies of 2.0, 4.0, and 4.5 keV. The electron beam current was about 1.5 mA. Neon was injected into the main chamber with equilibrium pressure at 1.00×10^{-5}Pa (75 nTorr).

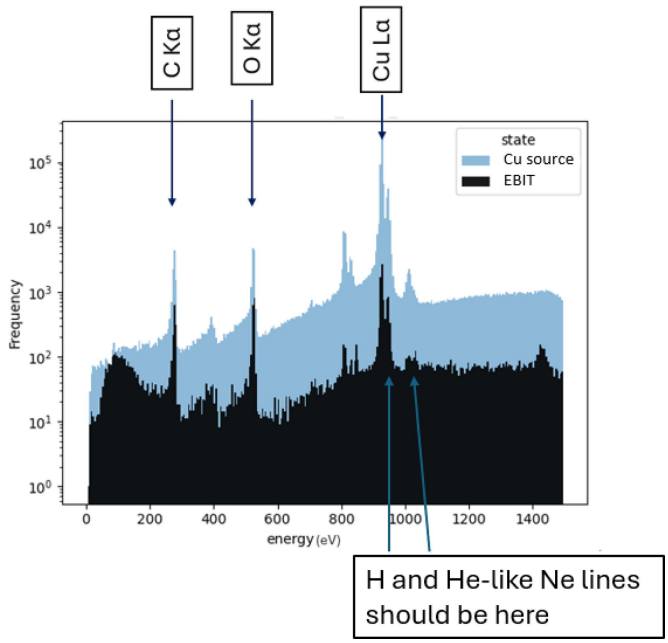

Fig. 7. X-ray emission spectra with the TES from a copper (Cu) calibration source (light blue) and the mini-EBIT with neon gas injection (black). Prominent characteristic emission lines for carbon (Kα), oxygen (Kα), and copper (Lα) are indicated by arrows.

that the Cu line is only visible from the port where the TES spectrometer is attached.

Although these TES arrays are in the initial stages of testing, an energy resolution of 1 eV FWHM at 900 eV has already been achieved. Our goal is to achieve $<$1 eV at 1.4 keV.

IV. Conclusion and Future Work

Highly charged ions have been successfully created and trapped inside the second-generation mini-EBIT, and X-rays were observed with the SDD. The TESs provided good energy resolution, proving their effectiveness in differentiating closely spaced emission lines. The pulsed gas injection system has also been assembled and bench-tested. It will be integrated into the mini-EBIT for further testing.

Further work will be done to optimize the mini-EBIT's operating parameters to efficiently produce and trap higher charged state ions that are of particular astrophysical interest. For future work, we also plan to attach the TES spectrometer to the current SDD port, which does not show the Cu line in the preliminary measurements, in order to help resolve the Cu Lα line overlap issue.

To minimize interference from the Bremsstrahlung background generated by the electron beam, it might be worth exploring the possibility of lowering the electron beam energy

below the ionization threshold or deflecting the beam to prevent further ionization of the gas and injecting the second neutral gas when the ions are magnetically confined, which is known as the "magnetic trapping" mode.

Once the system is calibrated and optimized, the primary goal is to perform detailed charge exchange measurements. In these measurements, neon ions will be trapped in the EBIT, and neutral helium will be introduced using the pulsed gas injection system, resolving individual lines from charge exchange transitions. The resulting X-ray emission will be recorded using the high-resolution TES, which is capable of resolving individual lines from charge exchange transitions. The resulting spectra will be analyzed to identify the emission lines, determine their cross sections, and compare them with theoretical predictions.

ACKNOWLEDGMENT

The authors would like to thank Joe Fowler and Jacob Ward for their useful feedback and comments.

REFERENCES

[1] R. K. Janev and H. Winter, "State-selective electron capture in atom-highly charged ion collisions," *Phys. Rep.*, vol. 117, no. 5–6, pp. 265–387, 1985.

[2] B. J. Wargelin, P. Beiersdorfer, and G. V. Brown, "EBIT charge-exchange measurements and astrophysical applications," *Can. J. Phys.*, vol. 86, no. 1, pp. 151–169, 2008.

[3] L. Gu and C. Shah, "Charge exchange in X-ray astrophysics," in *High-Resolution X-Ray Spectroscopy: Instrumentation, Data Analysis, and Science*. Singapore: Springer Nature Singapore, 2023, pp. 255–289.

[4] I. Kaganovich, A. Shnidman, H. Mebane, and R. Davidson, "Calculation of charge-changing cross-sections of ions or atoms colliding with fast ions using the classical trajectory method," *Nucl. Instrum. Methods Phys. Res. Sect. A: Accel., Spectrometers, Detectors Assoc. Equip.*, vol. 606, no. 1, pp. 196–204, 2009. [Online]. Available: https://www.sciencedirect.com/science/article/pii/S0168900209005762

[5] M. B. Shah, D. S. Elliott, and H. B. Gilbody, "Pulsed crossed-beam study of the ionisation of atomic hydrogen by electron impact," *J. Phys. B: At. Mol. Phys.*, vol. 20, no. 14, Jul. 1987, Art. no. 3501, doi: 10.1088/0022-3700/20/14/022.

[6] C. M. Lisse et al., "Discovery of X-ray and extreme ultraviolet emission from comet c/hyakutake 1996 b2," *Science*, vol. 274, no. 5285, pp. 205–209, 1996.

[7] T. E. Cravens, "Comet Hyakutake X-ray source: Charge transfer of solar wind heavy ions," *Geophysical Res. Lett.*, vol. 24, no. 1, pp. 105–108, 1997.

[8] K. Dennerl, "Discovery of x–rays from mars with Chandra," *Astron. Astrophys.*, vol. 394, no. 3, pp. 1119–1128, 2002, [Online]. Available: https://www.aanda.org/articles/aa/abs/2002/42/aa2918/aa2918.html

[9] K. Dennerl, V. Burwitz, J. Englhauser, C. Lisse, and S. Wolk, "Discovery of X–rays from venus with chandra," *Astron. Astrophys.*, vol. 386, no. 1, pp. 319–330, 2002, [Online]. Available: https://www.aanda.org/articles/aa/abs/2002/16/aa1955/aa1955.html

[10] D. M. Worrall, F. E. Marshall, E. A. Boldt, and J. H. Swank, "HEAO 1 measurements of the galactic ridge," *Astrophysical J.*, vol. 255, pp. 111–121, Apr. 1982.

[11] M. Revnivtsev, S. Sazonov, M. Gilfanov, E. Churazov, and R. Sunyaev, "Origin of the galactic ridge X-ray emission," *Astron. Astrophys.*, vol. 452, no. 1, pp. 169–178, 2006.

[12] P. Kaaret et al., "A disk-dominated and clumpy circumgalactic medium of the milky way seen in X-ray emission," *Nature Astron.*, vol. 4, no. 11, pp. 1072–1077, 2020.

[13] H. Pauls, G. Zank, and L. Williams, "Interaction of the solar wind with the local interstellar medium," *J. Geophysical Res.: Space Phys.*, vol. 100, no. A11, pp. 21595–21604, 1995.

[14] M. W. Wise and C. L. Sarazin, "Charge transfer and X-ray emission from supernova remnants," *Astrophysical J., Part 1 (ISSN 0004-637X)*, vol. 345, pp. 384–392, Oct. 1989.

[15] R. Fonck, "Charge exchange recombination spectroscopy as a plasma diagnostic tool (invited)," *Rev. Sci. Instrum.*, vol. 56, no. 5, pp. 885–889, 1985.

[16] R. Scott and J. Strachan, "Charge exchange spectroscopy for plasma diagnostics," *Nucl. Instrum. Methods Phys. Res. Sect. B: Beam Interact. Mater. At.*, vol. 10–11, pp. 473–477, 1985.

[17] K. Sato, Y. Uchida, and K. Ishikawa, "Hitomi/XRISM micro-calorimeter," in *High-Resolution X-Ray Spectroscopy: Instrumentation, Data Analysis, and Science*. Singapore: Springer Nature Singapore, 2023, pp. 93–123.

[18] M. S. Tashiro, "XRISM: X-ray imaging and spectroscopy mission," *Int. J. Modern Phys. D*, vol. 31, no. 02, Jan. 2022, Art. no. 2230001, [Online]. Available: https://www.worldscientific.com/doi/abs/10.1142/S0218271822300014

[19] European Space Agency, "ATHENA home - NewAthena mission overview," 2024, Accessed: Jul. 20, 2025. [Online]. Available: https://www.cosmos.esa.int/web/athena

[20] D. Barret et al., "The athena x-ray integral field unit: A consolidated design for the system requirement review of the preliminary definition phase," *Exp. Astron.*, vol. 56, pp. 213–266, 2023, [Online]. Available: https://research.rug.nl/files/714987309/s10686-022-09880-7.pdf

[21] S. F. Hoogerheide and J. N. Tan, "A miniature EBIT with ion extraction for isolating highly charged ions," *J. Phys.: Conf. Ser.*, vol. 583, 2015, Art. no. 012044, [Online]. Available: https://iopscience.iop.org/article/10.1088/1742-6596/583/1/012044

[22] J. Gillaspy, J. Roberts, C. Brown, and U. Feldman, "The NIST EBIT: A progress report," *AIP Conf. Proc.*, vol. 274, pp. 682–685, 1993.

[23] V. A. Yerokhin and V. M. Shabaev, "Lamb shift of n = 1 and n = 2 states of hydrogen-like atoms, $1 \leq z \leq 110$," *J. Phys. Chem. Reference Data*, vol. 44, no. 3, 2015, Art. no. 033103.

[24] A. C. Gall et al., "A cryogen-free electron beam ion trap for astrophysically relevant spectroscopic studies," Jan. 2024, *arXiv:2401.13088*.

[25] L. Schweikhard, P. Beiersdorfer, G. Brown, J. Crespo López-Urrutia, S. Utter, and K. Widmann, "Pulsed gas injection for X-ray spectroscopy of highly charged ions stored in the magnetic trapping mode of an electron beam ion trap," *Nucl. Instrum. Methods Phys. Res. Sect. B: Beam Interact. Mater. At.*, vol. 142, pp. 245–252, 1998.

[26] P. Szypryt et al., "A transition-edge sensor-based X-ray spectrometer for the study of highly charged ions at the national institute of standards and technology electron beam ion trap," *Rev. Sci. Instrum.*, vol. 90, no. 12, 2019, Art. no. 123107.

[27] J. C. Weber et al., "Development of a transition-edge sensor bilayer process providing new modalities for critical temperature control," *Superconductor Sci. Technol.*, vol. 33, no. 11, 2020, Art. no. 115002.